Am J Cancer Res 2023;13(11):5684-5697
www.ajcr.us /ISSN:2156-6976/ajcr0151847

Original Article

Tracking of trastuzumab resistance in patients with HER2-positive metastatic gastric cancer by CTC liquid biopsy

Jie Zhang[1*], Weiqing Qiu[1*], Wei Zhang[2*], Yuanwen Chen[1], Huojian Shen[1], Hongyi Zhu[1], Xiaofei Liang[3], Zhiyong Shen[1]

[1]Department of General Surgery, Renji Hospital, School of Medicine, Shanghai Jiaotong University, Shanghai, China; [2]Department of Gastroenterology and Hepatology, Renji Hospital, School of Medicine, Shanghai Jiaotong University, Shanghai, China; [3]Jukang (Shanghai) Biotechnology Co., LTD., Shanghai, China. [*]Equal contributors.

Received June 21, 2023; Accepted October 28, 2023; Epub November 15, 2023; Published November 30, 2023

Abstract: This study aimed to utilize circulating tumor cell-DNA (CTC-DNA) from liquid biopsies to monitor trastuzumab resistance in Gastric cancer (GC) and assess the limited response rate in HER2 metastatic gastric cancer. Given the heterogeneity of GC, we established a high-precision CTC detection system that effectively isolates tumor cells with high HER2 expression for downstream analysis. Targeted sequencing of 610 genes was conducted on 20 paired CTC and tissue samples to assess uniformity. A longitudinal analysis of CTC samples was then performed to monitor trastuzumab resistance throughout treatment. Targeted sequencing of the HER2 gene showed strong consistency with fluorescence in situ hybridization data. Detected HER2 Scna was superior in predicting tumor shrinkage and progression. Most patients with innate trastuzumab resistance exhibited elevated HER2 Scna levels during progression. PIK3CA mutations were significantly enriched, and ERBB2/4 gene mutations were predominant in patients with innate trastuzumab resistance. CTC-DNA sequencing provides new insights into gene alterations associated with trastuzumab resistance in HER2 mGC.

Keywords: Gastric cancer, HER2, trastuzumab, circulating tumor cell, NGS

Introduction

Gastric cancer (GC) is the fifth most commonly diagnosed cancer globally and the third leading cause of cancer-related deaths. However, advancements in GC treatment, especially in advanced stages, have been gradual [1, 2]. Human epidermal growth factor receptor 2 (HER2/ErbB2/neu) is a 185 kDa transmembrane receptor tyrosine kinase (RTK) and belongs to the epidermal growth factor receptor (EGFR) family [3-5]. HER2-positive GC constitutes approximately 6% to 30% of all GC cases. Given that overexpression of HER2 is observed in more than 15% of GC and is linked to a poor prognosis, it serves as a crucial therapeutic target for HER2-positive metastatic gastric cancer (mGC) [6, 7]. Currently, tissue detection is the primary diagnostic method. As biopsies provide limited information and can be invasive, there's a pressing need for non-invasive techniques to identify patients for anti-HER2 treatments and to monitor therapeutic outcomes, thereby improving the management of advanced GC [8, 9].

Over the last few decades, numerous studies have highlighted the potential of circulating tumor cells (CTCs) as a novel blood biomarker for the diagnosis, prognosis, and treatment of various cancers, including GC [10-12]. CTCs, tumor cells from primary or metastatic foci that are shed into the peripheral circulation, carry the genetic and phenotypic information of the parental lesion, and thus have high research and clinical value. Liquid biopsy with CTC detection as a diagnostic tool has been widely studied in its application to GC and has progressed from a simple counting tool, to allowing for genotyping and molecular diagnostics. CTC detection and capture can aid in determining the genetic profiles of tumor cells over time

without requiring a direct biopsy of the tumor mass. Wang and his colleagues performed the targeted sequencing of 146 clinically relevant genes in 78 paired plasma circulating tumor DNA (ctDNA) and biopsy samples to determine the consistency of plasma with tissue [13]. However, there are still gaps in comparing the consistency of DNA from CTC with tumor tissue. Since GC has high intrinsic molecular heterogeneity, the single-site immune lipid magnetic beads have a higher chance than multi-site beads to miss CTCs. Multi-site immune lipid magnetic beads based on HER2 and EpCAM can better capture CTCs of GC, improve the positive detection rate, and provide a foundation for the classification of GC and subsequent prognosis based on genetic signatures and CTC prevalence.

Trastuzumab, a targeted therapy for HER2, is effective both as a standalone treatment and in combination with other drugs. Evaluating GC tissues for HER2 overexpression is crucial to identify patients who would benefit from trastuzumab. Clinical trials have demonstrated that overall survival of HER2-positive GC patients significantly improved from trastuzumab treatment, leading to its approval as a first-line therapy [6]. Studies have shown that MET (hepatocyte growth factor receptor) mutations are present in GC patients, especially those with drug resistance. Some studies suggest that MET mutations contribute to resistance mechanisms against alfatinib and lapatinib in GC. We isolated GC CTCs using multi-site immune lipid magnetic beads targeting HER2 and EpCAM for early diagnosis and prognosis assessment. These captured CTCs were cultured to develop an animal model to study the impact of MET mutations on trastuzumab resistance in GC.

Materials and methods

Sample collection

Blood was collected from 50 patients, along with tissue samples of 20 paired patients, who had been pathologically diagnosed with GC in South Hospital of Renji Hospital, Shanghai Jiaotong University hospital between November 2020 and March 2022. All samples were obtained with informed patient consent, and the study was approved by the Ethics Committee of the Shanghai Jiaotong University Affiliated Renji Hospital (KY2021-013).

Materials and instruments

RPMI, fetal bovine serum (FBS), and trypsin were purchased from Gibco. BALB/C nude mice were purchased from Shanghai Jiesijie Laboratory Animal Co., Ltd. Anti-HER2 antibody (ab16901) and goat anti-rabbit secondary antibody (ab6721) were purchased from Abcam. The Path Vysion HER2 kit for fluorescence in situ hybridization (FISH) probe, RIPA lysate, and chemiluminescence kit were purchased from Shanghai Abbott Biotechnology Co., Ltd. 1-ethyl-3-(3-dimethylammonium propyl) ammonium carbohydrate (EDC), N-hydroxysuccinimide (NHS), EpCAM-lipid magnetic beads, Fe_3O_4, carboxymethyl chitosan hexadecane alkyl quaternary amine salt (HQCMC), 1,2-dioleoylphosphatidylcholine (DOPC) and dimethyl octadecyl epoxypropyl ammonium chloride (GHDC) were purchased from Huzhou Lieyuan Medical Laboratory Co., Ltd. OLYMPUS B×61 fluorescence microscope was purchased from Olympus Corp, a Japanese enterprise. BI-90Plus laser particle analyzer/Zeta potentiostat was purchased from American Brook Haven. XL-30 environmental scanning electron microscope (ESEM) was purchased from PHILIPS in the Netherlands.

Preparation of HER2- and EpCAM-lipid magnetic beads

HER2-lipid magnetic beads (H-LMB) and EpCAM-lipid magnetic beads (E-LMB) were synthesized as described in referenced literature. In brief, a mixture of cholesterol, DOPC, GHDC, HQCMC, and Fe_3O_4 in dichloromethane was combined with a 0.1 M PBS solution. The mixture was stirred vigorously to ensure emulsification and heated to 25°C to obtain LMBs. During this process, mechanical stirring was imperative to avoid agglomeration or aggregation of iron oxide nanoparticles and nanocolloids. 0.6 mg HER2 antibody was dissolved in 10 mL isopropanol. Coupling agents EDC and NHS were added respectively to the mixture of nanomagnetic beads. This mixture was stirred at a constant rate for 24 h to obtain lipid magnetic beads conjugated with anti-HER2 antibody. The preparation process for EpCAM-lipid magnetic beads was the same as above.

Characterization of HER2-LMB and Ep-LMB

10 μL H-LMB of the sample was diluted with 1 mL distilled water; a BI-90Plus laser particle

analyzer/Zeta potentiostat was then used to detect the particle size and zeta potential. The atomistic characteristics of H-LMB were determined by an atomic force microscope (AFM). 10 μL H-LMB sample was diluted with 1 mL distilled water. Then, 50 μL of this solution was coated on a mica sheet for working in non-contact tap mode (frequency =325 Hz) at a scanning speed of 1.0 Hz. The mica sheet was observed when it was dried. 10 μL H-LMB and LMB samples were diluted with 1 ml distilled water, respectively, after which the absorbance (A) at 280 nm was measured with an ultraviolet (UV) spectrophotometer. The magnetic property of H-LMB was detected with a vibrating sample magnetometer. The characterization of E-LMB was the same as above.

Detection of expression of HER2 in tissues of GC patients

HER2 expression in GC tissues was confirmed using FISH. Tissues were treated at high temperature and high pressure for 3 min, digested with pepsin (0.2 mg/ml) for 20-40 min, then dehydrated and dried. 10 mL probe mixture was added to the target region of tissue slices, which were then covered and sealed. Tissue slices were placed in an in situ hybridization instrument and denatured at 83°C for 5 min then hybridization was performed at 45°C overnight (14-18 h). Tissue slices were rinsed quickly and dried at room temperature. 15 μL DAPI was added dropwise, slices were sealed, and staining was observed under a fluorescence microscope.

Gene detection

Second-generation sequencing by ligation and bioinformatic analysis were performed by Daen Biotechnology Co., Ltd. The ligation reactions of 4 fluorescent-labeled oligonucleotides were used for sequencing. Before sequencing, the DNA template was concentrated by Integrated vacuum concentrator (BIONOON VAC-AIO, Shanghai BANNUO BIOBECHNOLOGY CO., LTD.) and amplified by emulsification PCR, and the 3'-modified microbeads were deposited on the glass substrate. Sequencing by ligation was performed using an 8-base fluorescent probe mixture. Multiple rounds of hybridization were performed where fluorescent probes matching the reverse complement template at the 5' end are ligated to the 3' end of the anchor sequence. DNA at these ligation positions can then be determined by fluorescent readout.

Statistical analysis

Data were processed using SPSS 20.0. Comparisons between groups were made using the independent samples t-test, with a significance threshold set at α=0.05. A *p*-value less than 0.05 was deemed statistically significant. All reported data represent the mean of three independent experiments.

Results

Procedures and characterization of LMB

In this study, we aimed to separate and identify CTCs from peripheral blood (PB) in GC clinical samples, perform quantitative statistics, and conduct genetic tests based on the established lipid magnetic beads for HER2 and other antibodies (including EpCAM lipid magnetic beads; E-LMB is a routine general-purpose CTC sorting system). This approach was chosen to investigate the ability of CTC capture to help detect and monitor trastuzumab resistance in GC. Technical details are illustrated in **Figure 1**.

The performance of nanomagnetic bead sorting in the CTC separation and detection system is paramount for high efficiency at capturing GC CTC in the blood. The UV absorption spectrum is shown in **Figure 2A**. The nanolipid magnetic beads for HER2 antibody and EpCAM antibody exhibited distinct UV absorption peaks near 280 nm, indicating the presence of modified antibodies on the nano magnetic bead surface, and that antibody loading was controllable. **Figure 2B** shows the magnetic saturation curve for E-LMB and H-LMB, with empty LMB serving as the control. The results confirmed that the prepared magnetic beads possess high saturation magnetization and superparamagnetism. The saturation magnetization of E-LMB and H-LMB at 300k was 18.97 emu/g, which was about 73.4% of that of raw Fe_3O_4 magnetic beads. The particle size distribution diagram for E-LMB and H-LMB is displayed in **Figure 2C** and **2E**, respectively. The average particle size was 204.1±5.7 nm and 193.7±6.4 nm, respectively. These findings were similar to the results of particle size shown by AFM (**Figure 2G**, **2H**). The surface potentials of E-LMB and H-LMB were 19.4±3.1 mV and 25.8±2.6 mV in a neu-

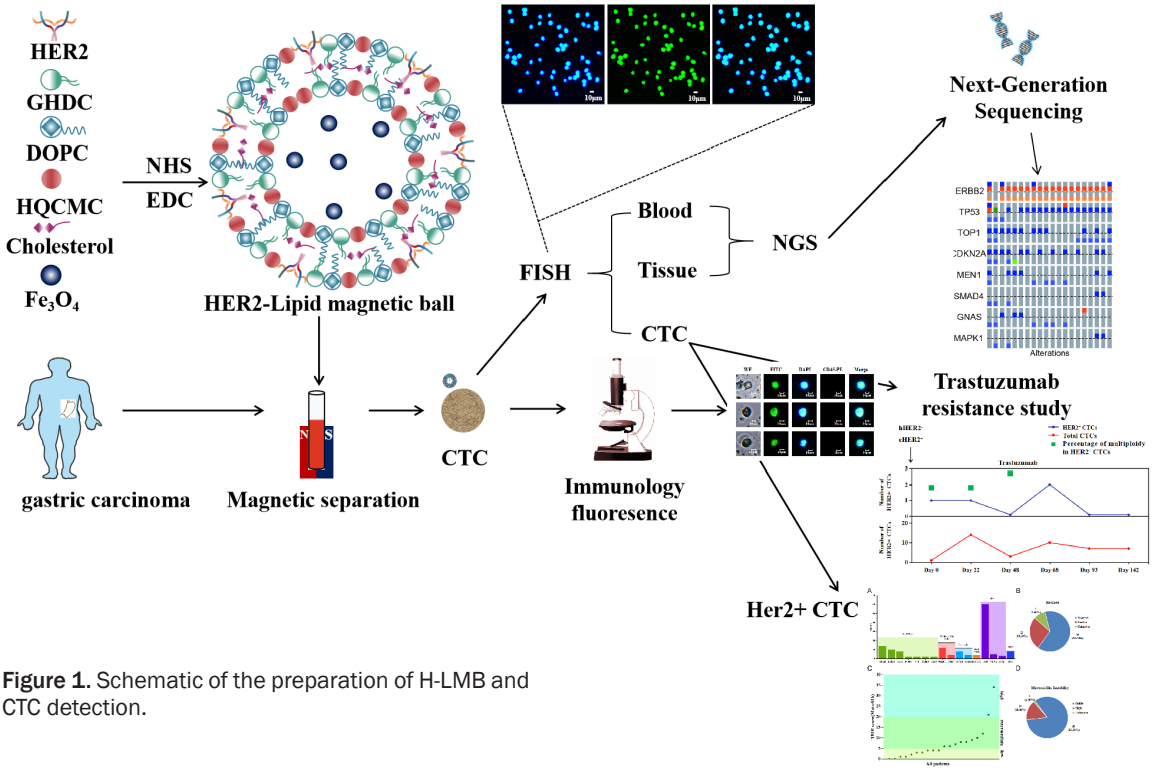

Figure 1. Schematic of the preparation of H-LMB and CTC detection.

tral state, which reduces the nonspecific adsorption interference observed in previous studies (**Figure 2D**, **2F**). These characterizations confirm the successful construction of the E-LMB and H-LMB capture systems for GC CTCs.

CTC detection and FISH

Since HER2 overexpression is the main marker of HER2+ GC, we analyzed CTC captured by H-LMB using FISH. Immunofluorescence characterization of CTC captured by E-LMB and H-LMB is shown in **Figure 3A**. GC patient CTCs exhibited distinct cellular morphology under white light and were strongly positive for CK19-FITC green fluorescence and DAPI blue luminescence. Captured cells were determined to be GC CTC by HER2+CK19+CD45- staining. FISH was used to analyze the blood of 20 GC patients. HER2 mutations were detected in the CTCs separated from the tissues of 5 GC patients and captured from 6 H-LMBs. Among 20 GC patient blood samples, 7 cases exhibited HER2 mutations, with 6 patients having CTCs with HER2 mutations. A subset of the detection results is presented in **Figure 3B** (refer to **Table 1** for patient details).

To achieve precise labeling for both IF and FISH, we meticulously optimized the procedure to ensure effective labeling for both targets. All conditions, including temperature, duration, and reagent concentration, were refined through preliminary experiments using cell line-spiked peripheral blood (**Figure 4**). Specifically designed for the HER2 gene amplification, the FISH method was employed, and the results of the analysis of mean HER2 copy number/cell, mean CEP17 copy number/cell, and mean HER2 copy number/mean CEP17 copy number are presented in Figure S1. The results revealed that mean HER2 copy number/cell was the highest, while mean CEP17 copy number/cell was the second highest, and mean HER2 copy number/mean CEP17 copy number was the lowest.

Molecular alterations in tumor and fluid biopsies of GC patients

To assess the consistency between molecular alterations detected in tumor and fluid biopsies, we sequenced 610 genes in 20 GC patients (14 CTC HER2+ and 6 CTC HER2-) and analyzed DNA copy number alterations, mutations, and structural variations in the tumor tis-

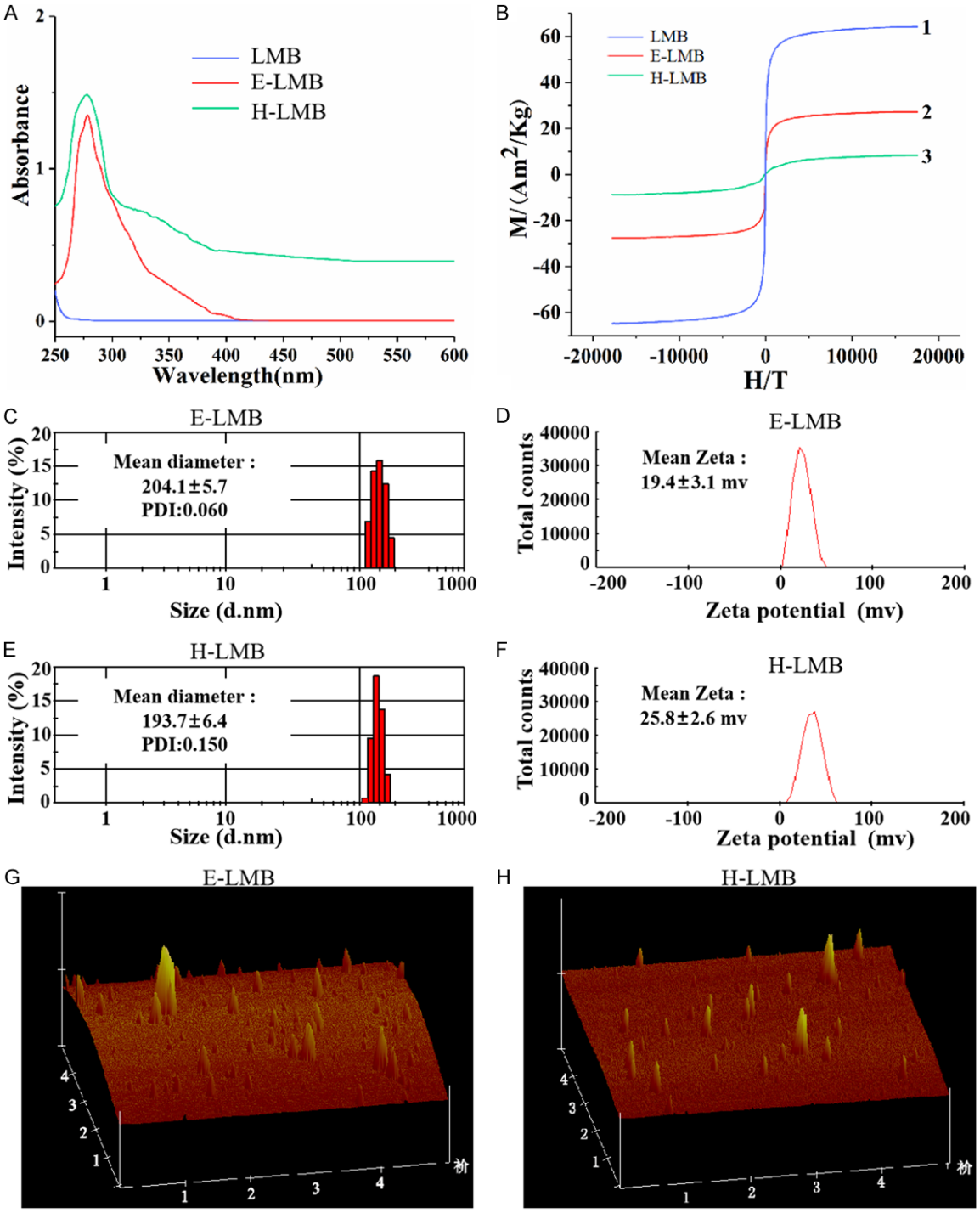

Figure 2. A. UV absorption spectrum of E-LMB and H-LMB; B. Magnetic saturation curve of E-LMB and H-LMB; C-F. Zeta-potential distribution and particle size distribution of E-LMB and H-LMB; G, H. Atomic force image of E-LMB and H-LMB.

sues of 20 patients paired with regular PB (detailed data of the 610 genes is provided in Table S1). **Figure 5A** displays the high-frequency (> 5%) molecular alterations detected in tissues and blood. The results revealed that ERBB2 (HER2) and TP53 are the most frequently altered genes in both tissues and blood, exhibiting notable heterogeneity. In

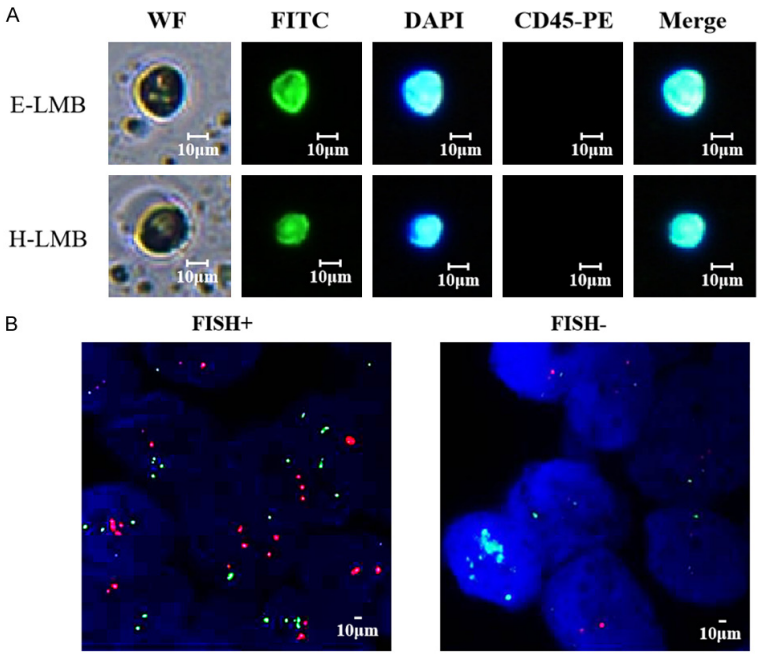

Figure 3. (A) Immunofluorescence identification results of CTCs of GC patients captured by E-LMB and H-LMB; and (B) FISH detection results of HER2 mutations in tissues of GC patients.

Table 1. Clinical information and CTC count of patients

ID	Gender	Age	Tumor staging	CTC (+/-)
17201425	Male	55	II	6
17200334	Male	60	III	3
20117667	Male	71	IV	3
17201248	Female	65	I	2
17106909	Male	64	III	11
17102754	Male	52	III	12
17201002	Male	48	II	6
17202979	Female	68	IV	13
18201228	Male	49	I	4
20088540	Male	74	I	3
18201228	Male	49	II	10
18202862	Male	55	III	11
18202832	Male	55	III	6
19200731	Female	72	II	9
18201695	Female	64	III	8
19201069	Male	68	IV	17
17201866	Male	65	II	9
19200731	Female	72	III	11
19201326	Female	58	I	3
19201069	Male	68	II	6

terms of mutation identification, tissue-based detection methods generally identify more mutations. However, the number of mutations detected in tissues and CTC samples is highly correlated. Although the overall consistency was low, we observed increased consistency with advancing stages. Specifically, the detection ratio of TP53/HER2 mutation consistency between mGC (stage) tissues and CTC samples was 71.43% (**Table 2**). In conclusion, the molecular alterations detected in CTCs accurately reflect the state of tumor tissues, especially in advanced stages.

We defined molecular alterations associated with trastuzumab resistance as an increase in mutations or mutation during treatment. As depicted in **Figure 5B**, in 6 (76.5%) patients, the molecular alterations of these genes abruptly changed or mutated during treatment, potentially indicating trastuzumab resistance.

Considering the benefits of a larger sample size, we analyzed the sequencing results of 33 additional gastric cancer CTC-NGS to identify the primary CTC-derived mutant genes in gastric cancer. The results are presented in Figure S2C, which highlights several genes with high mutation frequency, including TP53, ERBB2, and CDH1. We also enumerated the primary mutation sites for these genes, as shown in Figure S2A, S2B, S2D, S2E. The primary mutation sites of TP53 were exon 5, exon 6, exon 7, and exon 8. The primary mutation sites of ERBB2 (HER2) were exon 3, exon 17, exon 20, exon 21, exon 22, and exon 26. The primary mutation sites of ARID1A were exon 1, exon 12, exon 18, and exon 20.

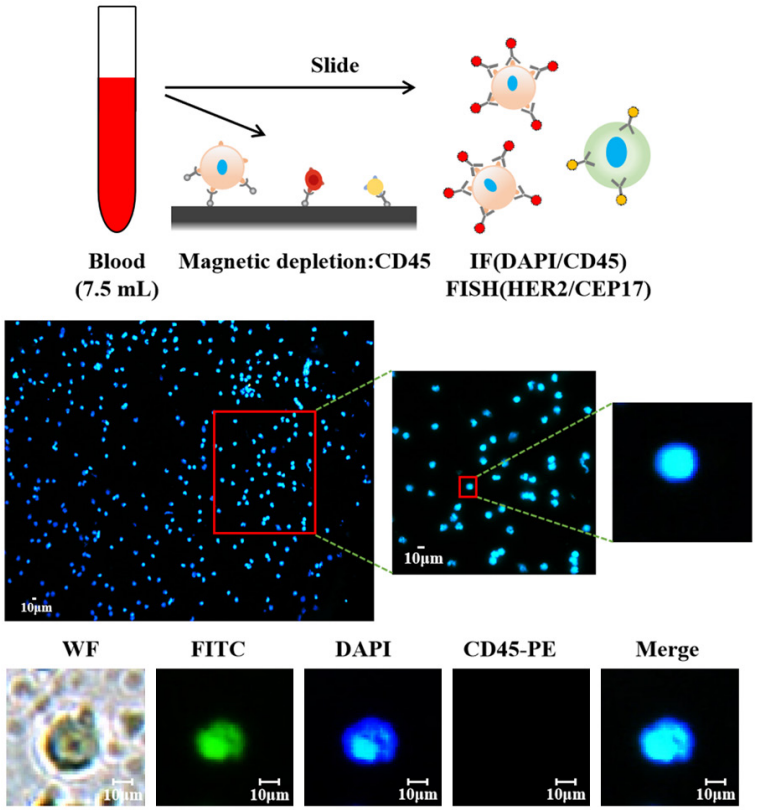

Figure 4. Immunofluorescence and FISH labeling in immunomagnetically enriched tumor cells: schematic of the specimen preparation and fluorescent labeling.

The primary mutation sites of CDH1 were exon 2, exon 4, exon 8, and exon 16.

HER2 amplification in trastuzumab resistance

Of the enrolled patients, 16 had been treated with trastuzumab, while 9 were currently undergoing trastuzumab treatment. Among the 10 patients showing progression, 9 exhibited secondary resistance (PFS > 3 months), and 6 displayed primary resistance (PFS ≤ 3 months). **Figure 6A** demonstrates that the HER2 copy number and mutation number correlate strongly with tumor load and outperform CEA and CTC count in predicting tumor shrinkage. Since tumor heterogeneity plays a crucial role in resistance and HER2-amplified subclones are preferentially targeted by trastuzumab, we analyzed the potential progression of trastuzumab-resistant clones (**Figure 6B**). Among advanced GC patients, HER2 amplification was detected in 10 patients (59%) at both baseline and the PD stage. These patients might develop resistant clones from HER2 amplification, thereby overcoming trastuzumab treatment, which require tailored therapeutic regimens (**Figure 6C**). In another 4 patients (23%), HER2 amplification was detected at baseline but not during PD, suggesting that trastuzumab treatment might have eliminated HER2 amplification and clones, with resistance driven by other non-HER2 amplified clones (**Figure 6D**). Tracking of enrolled samples revealed changes in CTC number from Baseline to PR to SD to PD. The results indicated a decrease in CTC number during the transition from Baseline to PD (Figure S3A-C), followed by a slight increase (Figure S3D-F), and then a substantial increase (Figure S3G-I).

Identification of patients with different resistance by CTC-DNA analysis

The total number of GC CTCs captured by conventional EpCAM magnetic beads and Vimentin magnetic beads was slightly higher than that captured by HER2 magnetic beads (**Figure 7A**). However, HER2 magnetic beads do have advantages in capturing GC CTCs. With further optimization in relation to variations in sample size and the distribution of enrolled patient stages, the capture efficiency of HER2 lipid magnetic beads for GC CTCs is expected to improve. ERBB2 amplification, along with ERBB2 amplification combined with PIK3CA/R1/C3 mutations, were the most common changes associated with trastuzumab resistance (**Figure 7B**). Specifically, PIK3CA mutations were more prevalent in patients with innate resistance (2/3, 66.6%) (**Figure 7B**), suggesting that detecting PIK3CA mutations may be an important biomarker to determine innate resistance.

We reviewed additional clinical samples performing CTC counting and typing, with results summarized in Figure S4. The findings were consistent with the above trend: the number of GC CTCs captured by conventional EpCAM

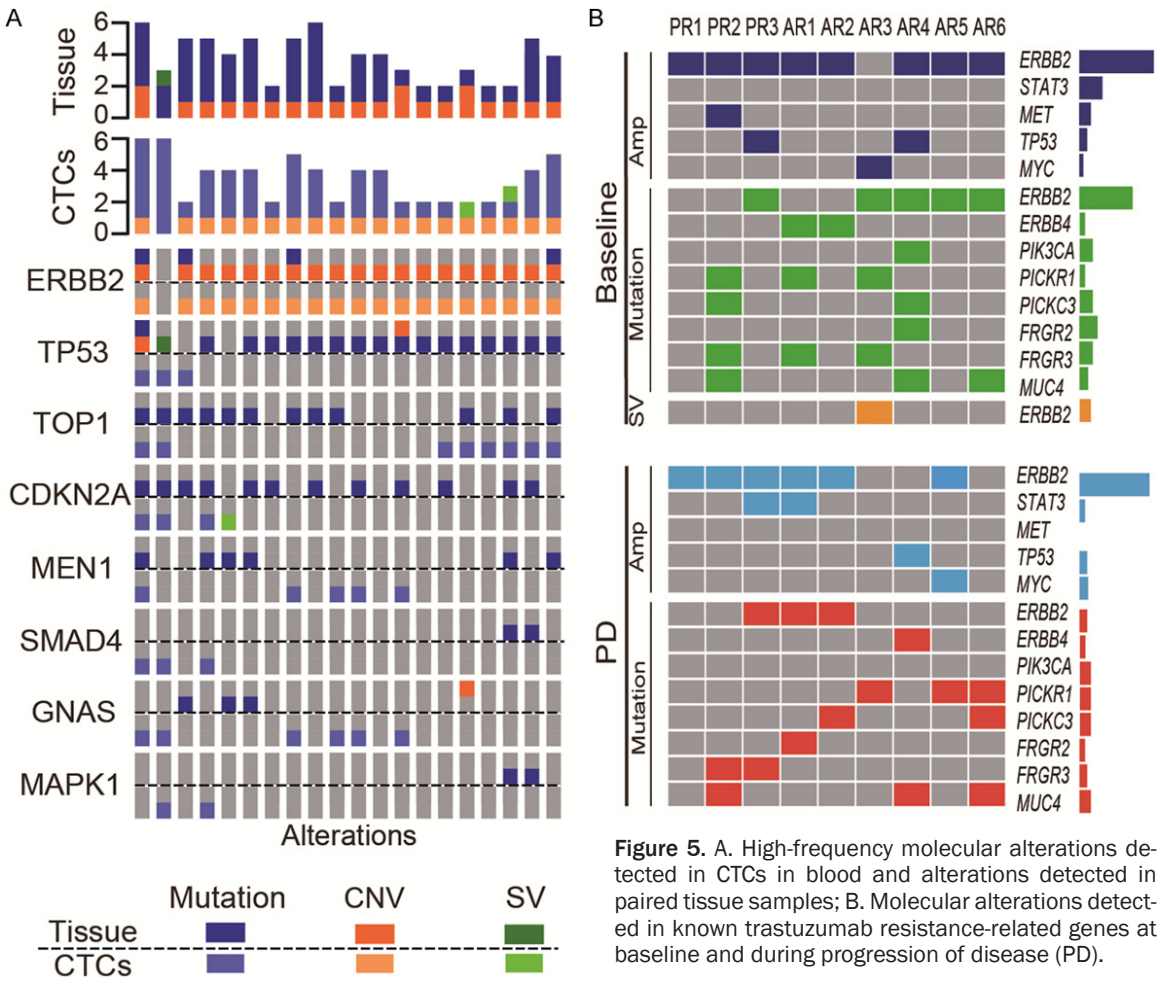

Figure 5. A. High-frequency molecular alterations detected in CTCs in blood and alterations detected in paired tissue samples; B. Molecular alterations detected in known trastuzumab resistance-related genes at baseline and during progression of disease (PD).

Table 2. The clinicopathological characteristics of patients (N=50)

Characteristics Number		TP53+		HER2+	
		tissue	CTC	tissue	CTC
Gender					
Male	39	16	9	18	13
Female	11	10	10	11	11
Age					
<65	38	21	13	24	19
≥65	12	10	6	5	6
Tumor Stage					
I Stage	8	5	6	4	4
II Stage	5	4	2	4	1
III Stage	16	14	10	15	13
IV Stage	11	8	7	6	7
Trastuzumab treatment					
Yes	32	18	12	26	24
No	18	13	7	3	1

beads and Vimentin beads was slightly higher than that captured by HER2 beads.

Distribution of microsatellite status and gene mutation

CTC-DNA carries information on tumor molecular biology. High-throughput sequencing of CTC-DNA can reflect tumor TMB values and microsatellite stability. Summarized TMB values and gene mutations in CTC-NGS data are summarized in **Figure 8**. Specific gene mutation results are presented in **Figure 8A**, **8B**, with the frequency of each gene mutation represented by the bar chart's height. HER2 mutations are further delineated in **Figure 8B**. Among the evaluated GC patients, 11 (15.3%)

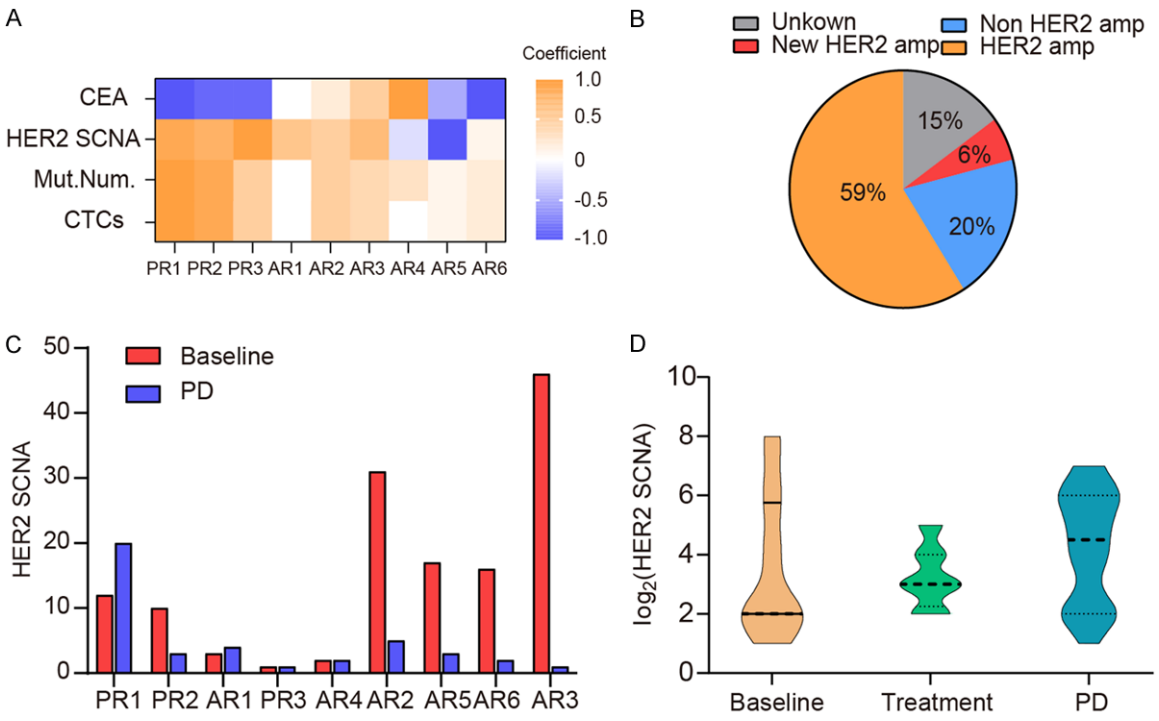

Figure 6. (A) Consistency between tumor load and CEA, HER2 SCNA, Mutation Load, and CTC count indicators; (B) Distribution of potential trastuzumab resistance clones in tumor progression; (C) Copy number of HER2 detected at Baseline, during Treatment and during PD; and (D) Copy number of HER2 detected at Baseline and during PD.

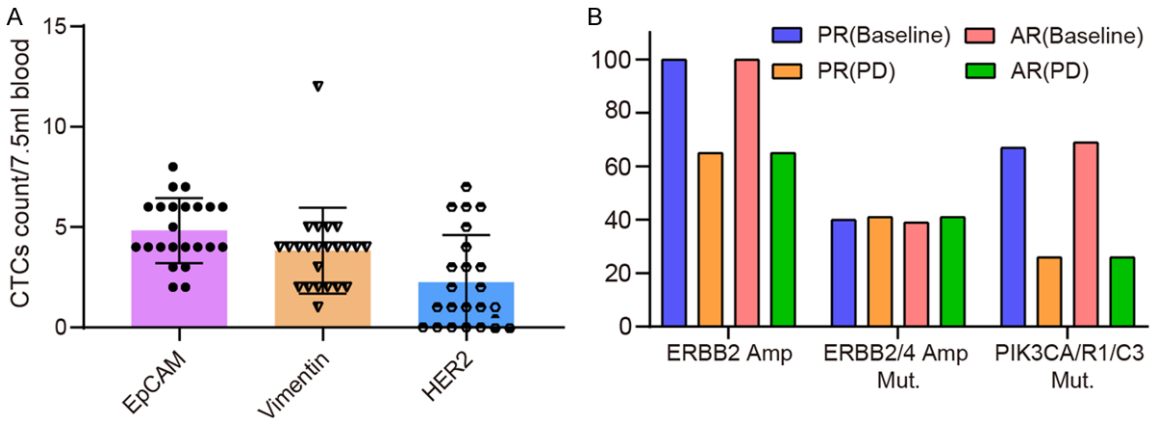

Figure 7. A. Number of CTCs captured from blood; B. Changes in ERBB2/4 and PIK3CA/R1/C3.

were microsatellite instable (MSI), while 60 patients (83.3%) were microsatellite stable (MSS) (**Figure 8D**). Specific TMB values are shown in **Figure 8C**.

Effect of trastuzumab drug on gastric cancer cells

Given that GC samples with abnormal HER2 expression/mutation are currently targeted for disease remission using trastuzumab, we analyzed the functional impact of trastuzumab on GC cells in NCI-N87 and MGC803. After optimizing trastuzumab concentration, we found that cell proliferation significantly decreased at concentrations exceeding 25 μg/mL, while trastuzumab-resistant cell lines were less affected by trastuzumab concentration (**Figure 9A**, **9B**). We also investigated the effects of trastuzumab on the invasive ability and apopto-

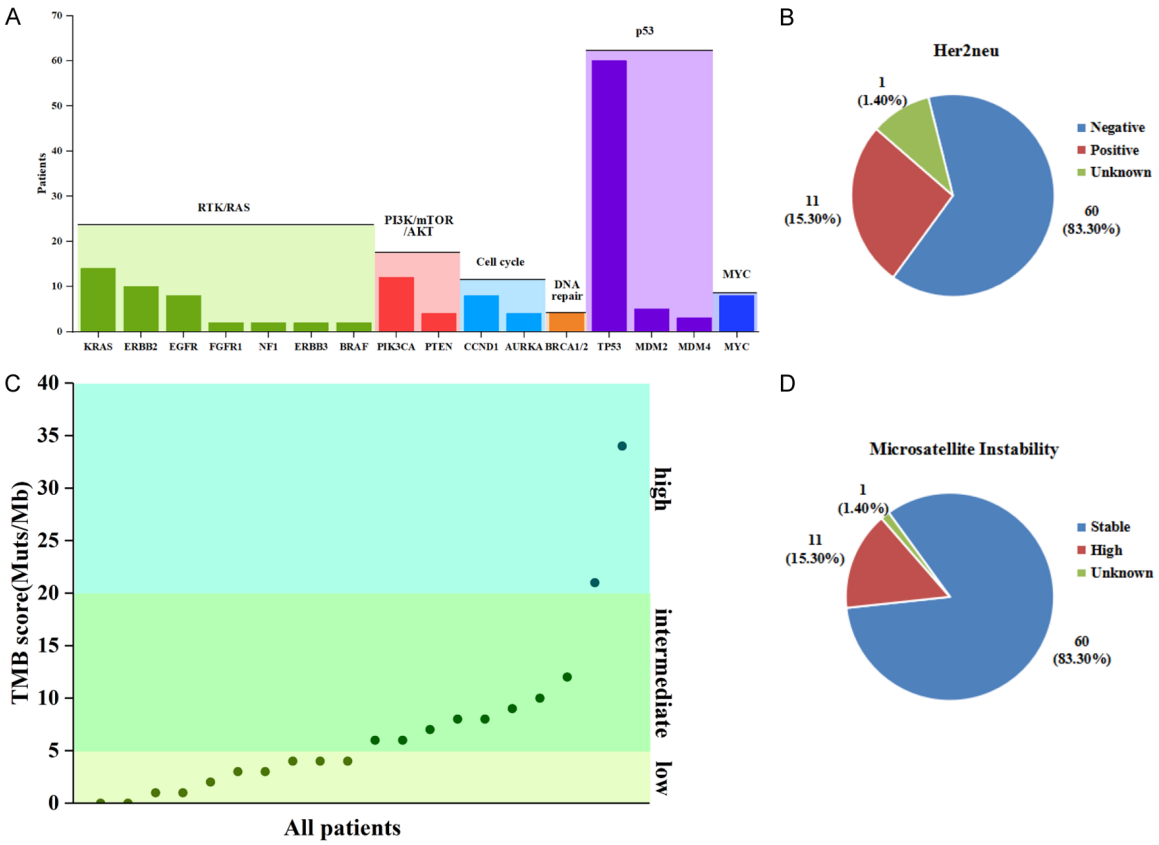

Figure 8. A, B. Gene mutations in CTC-NGS sequencing data and specific results of HER2. C, D. Distribution of microsatellite status in CTC-NGS sequencing.

sis of GC cells at appropriate trastuzumab concentrations. The results revealed that the invasive ability of sensitive GC cells increased while their apoptotic ability decreased (**Figure 9C**, **9D**). In contrast, the invasive ability of resistant GC cells decreased, and their apoptotic ability increased (**Figure 9C**, **9D**). These findings suggest that trastuzumab interferes with GC cells. We also analyzed the proliferative capacity of GC cells in response to two other drugs (pyrotinib and apatinib), as shown in Figure S5. We further assessed changes in the proliferative capacity of GC cells after TPR-HER2, V10920, G10630, D12028, D12028, D12308, and Y12003 point mutations at seven drug concentrations.

Differential gene expression analysis

The workflow for gene expression analysis, including the identification and validation of candidate biomarkers under trastuzumab treatment, is presented in **Figure 10A**. Regulated genes and biomarker candidates were identified following gene expression analysis. Biomarker candidates were validated in vitro or clinical specimens. The expressions of three biomarkers, ERBB2, ERBB4, and PIK3CA, in GC cell lines (NCI-N87) are depicted in **Figure 10B-D**. The expressions of these three biomarkers in clinical specimens are shown in **Figure 10E**.

Discussion

Since GC is characterized by genomic heterogeneity, the clonal complexity of patients with multi-metastatic disease cannot be fully assessed by sampling from a single disease site due to its inherent complexity [14]. Recently, “liquid biopsies”, composed partially of CTCs, have emerged as a focal point in cancer research. CTCs hold significant clinical value in monitoring therapeutic responses and prognosticating disease outcomes [15, 16]. Consequently, CTC-DNA is instrumental in detecting genomic alterations across heteroge-

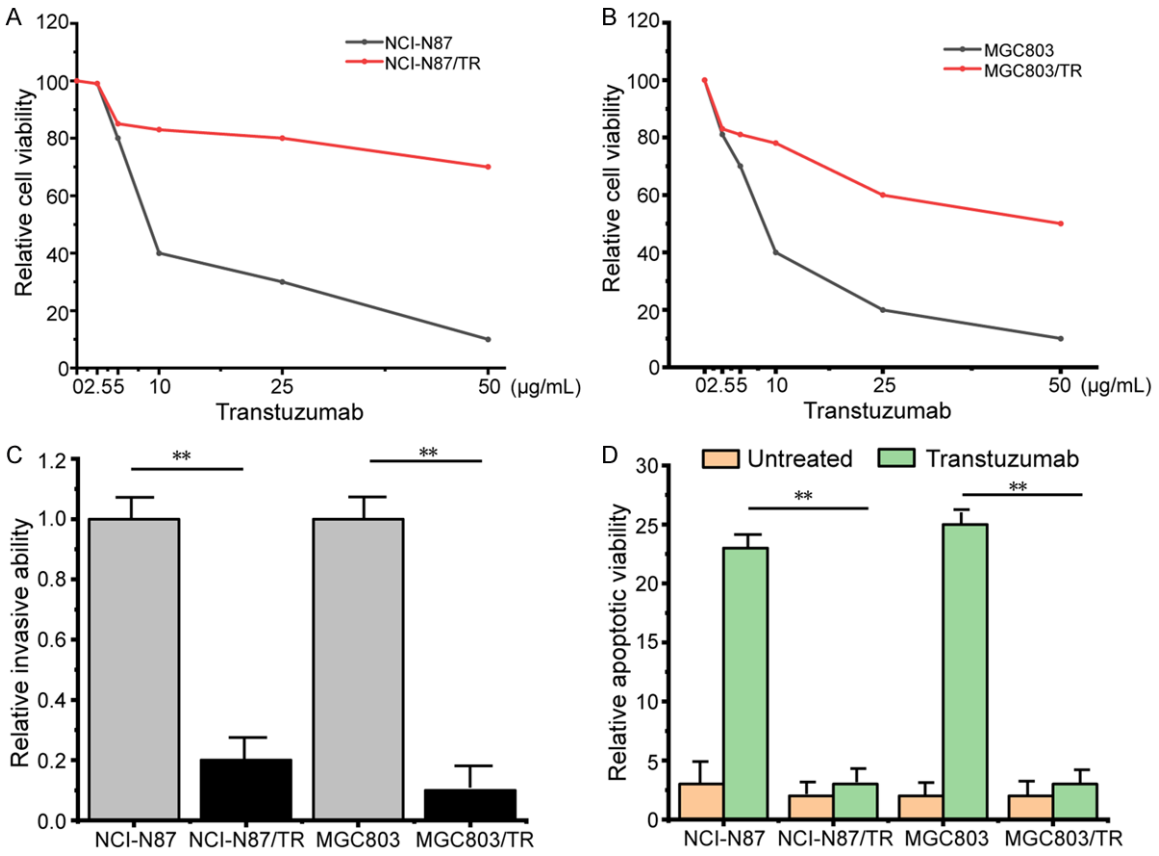

Figure 9. Determination of trastuzumab kill curve for GC cells: (A) NCI-N87, (B) MGC803. The effects of trastuzumab on the invasiveness (C) and apoptosis (D) of GC cells.

neous genomic sites. This study leverages a GC-CTC sorting system for drug resistance analysis and monitoring disease progression. To enhance GC-CTC enrichment, we constructed a specific HER2-LMB tailored for capturing GC-CTC.

Prior research has demonstrated the utility of CTC-DNA for monitoring resistance and investigating mechanisms in malignant tumors. However, the background noise from cell-free DNA (cfDNA) can limit the detection sensitivity of CTC-DNA [17]. Shoda and his colleagues successfully detected the HER2 copy number using ctDNA-based ddPCR [18]. Subsequently, Wang et al. utilized high-throughput sequencing for ctDNA genotyping, demonstrating the efficacy of this technique in monitoring trastuzumab resistance and pinpointing resistance emergence [13]. Extracting DNA from CTCs and employing next-generation sequencing (NGS) technology offer a promising avenue for dynamic resistance monitoring [19]. At the time of our study, of the patients examined, 16 had undergone trastuzumab treatment, while 9 were currently receiving treatment. Among the 10 patients showing progression, 9 exhibited secondary resistance (PFS > 3 months), and 6 displayed primary resistance (PFS ≤ 3 months). Furthermore, our analysis of high-frequency (> 5%) molecular alterations in tissues and blood revealed that ERBB2 (HER2) and TP53 are the most commonly altered genes, exhibiting pronounced heterogeneity.

The advent of NGS has significantly advanced our understanding of tumor molecular characteristics. Genome projects like the Cancer Genome Atlas Network and the Asian Cancer Research Group (ACRG) have greatly contributed to our molecular understanding of GC [20, 21]. Presently, NGS-based CTC-DNA genotyping has been validated as an effective method for monitoring trastuzumab resistance and discerning the resistance mechanisms in HER2+ GC [13, 22]. Our findings suggest that CTC-DNA can predict trastuzumab responses, with the persistence or resurgence of HER2-amplified

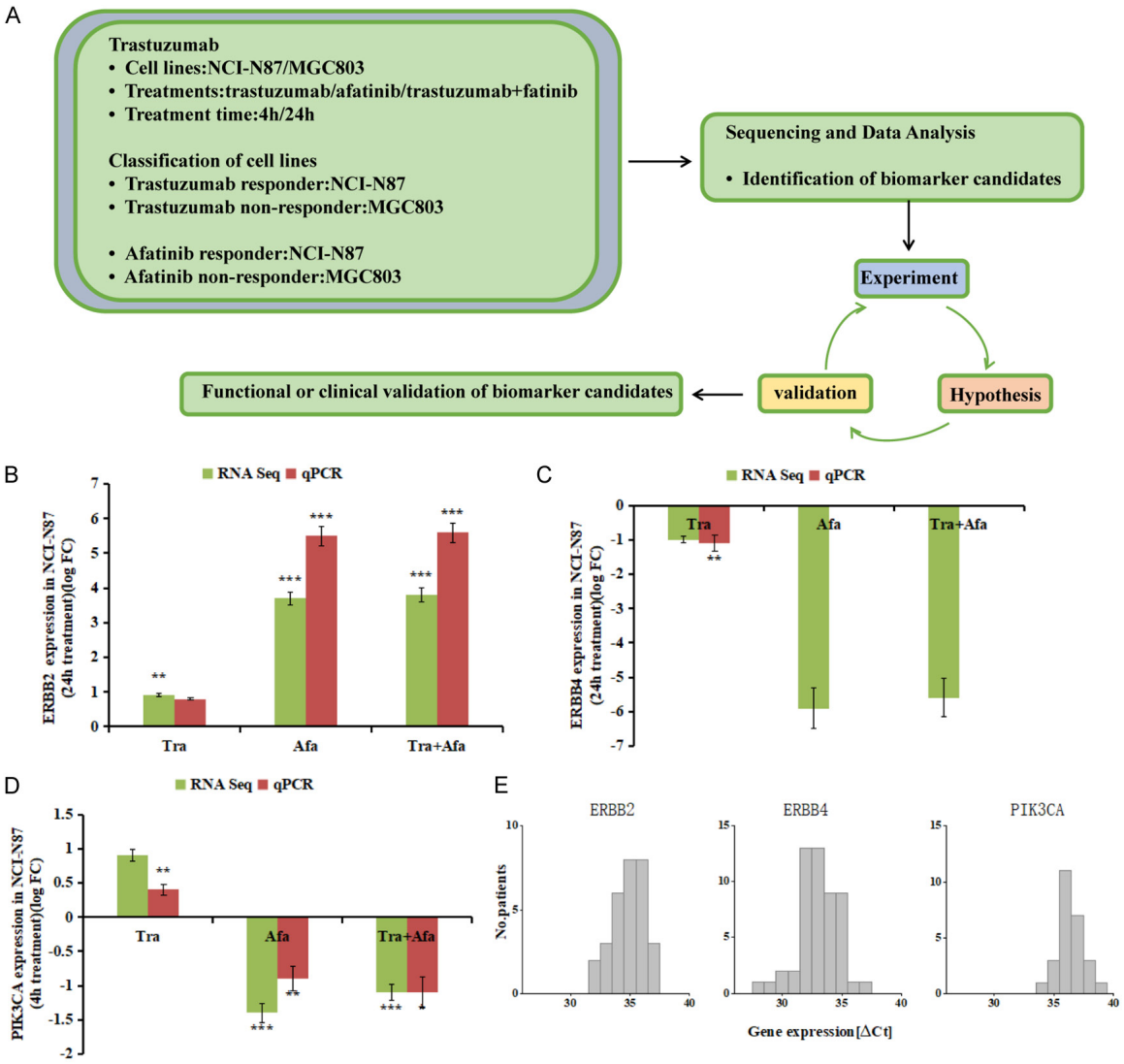

Figure 10. A. The workflow for gene expression analysis of candidate biomarkers under trastuzumab treatment. B-D. The expressions of ERBB2, ERBB4 and PIK3CA in NCI-N87 cell lines. E. The expressions of ERBB2, ERBB4 and PIK3CA in GC clinical specimens.

copies in blood signaling tumor progression linked to resistance. In our NGS-based CTC-DNA analysis, we identified multiple resistance mechanisms in 76.5% of patients. Notably, patients exhibiting multiple resistance mechanisms (PIK3CA/R1/C3 and ERBB2/4) experienced a significant reduction in progression-free survival (PFS) post-trastuzumab treatment. These findings underscore the potential of isolated CTC-DNA to effectively reflect the non-heterogeneity of acquired resistance mechanisms.

Recently, CTCs have garnered global attention as a means to surmount the challenges posed by the inherent limitations of tissue samples [23, 24]. While CTC-DNA profiling may offer valuable insights into potential molecular changes associated with trastuzumab resistance, this technique has its limitations [25-27]. For instance, although our 610-gene panel encompasses most genes linked to solid tumors, there might be mutations in genes outside our panel. Additionally, gene functions regulated at transcriptional, translational, or post-translational levels might evade detection by DNA sequencing. The low abundance of CTCs in blood also poses challenges, as other cells might be inadvertently captured, potentially skewing detection results. However, the

mechanism of CTC capture allows for the identification of proteins along with the co-localization of nucleic acid sequences by staining, demonstrating the techniques' potential in resistance research. Moreover, our comprehensive analysis of cell biological functions in GC cell lines has provided further insights. By tracking and monitoring trastuzumab resistance in GC and focusing on HER2 (mGC) using CTC-DNA from 20 GC patient samples, we have highlighted the significance of CTC analysis in understanding disease heterogeneity, clonal evolution, and clonal dynamics.

Acknowledgements

This study was supported by the Natural Science Foundation of Shanghai (20ZR1433300).

Written informed consent was obtained from patient.

Disclosure of conflict of interest

The author Xiaofei Liang is employed by Jukang (Shanghai) Biotechnology Co., LTD. The remaining authors declare that the research was conducted in the absence of any commercial or financial relationships that could be construed as a potential conflict of interest.

Address correspondence to: Zhiyong Shen and Hongyi Zhu, Department of General Surgery, Renji Hospital, School of Medicine, Shanghai Jiaotong University, No. 2000, Jiangyue Rd., Shanghai 201100, China. E-mail: doctor_szy7089@163.com (ZYS); rj_zhuhongyi@163.com (HYZ); Xiaofei Liang, Jukang (Shanghai) Biotechnology Co., LTD., No. 28, Xiangle Rd., Shanghai 201800, China. E-mail: xfliang86@126.com

References

[1] Castelli G, Pelosi E and Testa U. Liver cancer: molecular characterization, clonal evolution and cancer stem cells. Cancers (Basel) 2017; 9: 127.

[2] Ho SWT and Tan P. Dissection of gastric cancer heterogeneity for precision oncology. Cancer Sci 2019; 110: 3405-3414.

[3] Gravalos C and Jimeno A. HER2 in gastric cancer: a new prognostic factor and a novel therapeutic target. Ann Oncol 2008; 19: 1523-9.

[4] Doi T, Shitara K, Naito Y, Shimomura A, Fujiwara Y, Yonemori K, Shimizu C, Shimoi T, Kuboki Y, Matsubara N, Kitano A, Jikoh T, Lee C, Fujisaki Y, Ogitani Y, Yver A and Tamura K. Safety, pharmacokinetics, and antitumour activity of trastuzumab deruxtecan (DS-8201), a HER2-targeting antibody-drug conjugate, in patients with advanced breast and gastric or gastro-oesophageal tumours: a phase 1 dose-escalation study. Lancet Oncol 2017; 18: 1512-1522.

[5] Seo S, Ryu MH, Park YS, Ahn JY, Park Y, Park SR, Ryoo BY, Lee GH, Jung HY and Kang YK. Loss of HER2 positivity after anti-HER2 chemotherapy in HER2-positive gastric cancer patients: results of the GASTric cancer HER2 reassessment study 3 (GASTHER3). Gastric Cancer 2019; 22: 527-535.

[6] Bang YJ, Van Cutsem E, Feyereislova A, Chung HC, Shen L, Sawaki A, Lordick F, Ohtsu A, Omuro Y, Satoh T, Aprile G, Kulikov E, Hill J, Lehle M, Rüschoff J and Kang YK; ToGA Trial Investigators. Trastuzumab in combination with chemotherapy versus chemotherapy alone for treatment of HER2-positive advanced gastric or gastro-oesophageal junction cancer (ToGA): a phase 3, open-label, randomised controlled trial. Lancet 2010; 376: 687-97.

[7] Tabernero J, Hoff PM, Shen L, Ohtsu A, Shah MA, Cheng K, Song C, Wu H, Eng-Wong J, Kim K and Kang YK. Pertuzumab plus trastuzumab and chemotherapy for HER2-positive metastatic gastric or gastro-oesophageal junction cancer (JACOB): final analysis of a double-blind, randomised, placebo-controlled phase 3 study. Lancet Oncol 2018; 19: 1372-1384.

[8] Grillo F, Fassan M, Sarocchi F, Fiocca R and Mastracci L. HER2 heterogeneity in gastric/gastroesophageal cancers: from benchside to practice. World J Gastroenterol 2016; 22: 5879-87.

[9] Kanayama K, Imai H, Yoneda M, Hirokawa YS and Shiraishi T. Significant intratumoral heterogeneity of human epidermal growth factor receptor 2 status in gastric cancer: a comparative study of immunohistochemistry, FISH, and dual-color in situ hybridization. Cancer Sci 2016; 107: 536-42.

[10] Alix-Panabières C and Pantel K. Circulating tumor cells: liquid biopsy of cancer. Clin Chem 2013; 59: 110-118.

[11] Castro-Giner F and Aceto N. Tracking cancer progression: from circulating tumor cells to metastasis. Genome Med 2020; 12: 31.

[12] Yamada T, Matsuda A, Koizumi M, Shinji S, Takahashi G, Iwai T, Takeda K, Ueda K, Yokoyama Y, Hara K, Hotta M, Matsumoto S and Yoshida H. Liquid biopsy for the management of patients with colorectal cancer. Digestion 2019; 99: 39-45.

[13] Wang DS, Liu ZX, Lu YX, Bao H, Wu X, Zeng ZL, Liu Z, Zhao Q, He CY, Lu JH, Wang ZQ, Qiu MZ,

Wang F, Wang FH, Li YH, Wang XN, Xie D, Jia WH, Shao YW and Xu RH. Liquid biopsies to track trastuzumab resistance in metastatic HER2-positive gastric cancer. Gut 2019; 68: 1152-1161.

[14] Kim SY. Cancer energy metabolism: shutting power off cancer factory. Biomol Ther (Seoul) 2018; 26: 39-44.

[15] Yang H, Li Y and Hu B. Potential role of mitochondria in gastric cancer detection: fission and glycolysis. Oncol Lett 2021; 21: 439.

[16] Qiu MZ, Li Q, Wang ZQ, Liu TS, Liu Q, Wei XL, Jin Y, Wang DS, Ren C, Bai L, Zhang DS, Wang FH, Li YH and Xu RH. HER2-positive patients receiving trastuzumab treatment have a comparable prognosis with HER2-negative advanced gastric cancer patients: a prospective cohort observation. Int J Cancer 2014; 134: 2468-77.

[17] Hurvitz SA, Andre F, Jiang Z, Shao Z, Mano MS, Neciosup SP, Tseng LM, Zhang Q, Shen K, Liu D, Dreosti LM, Burris HA, Toi M, Buyse ME, Cabaribere D, Lindsay MA, Rao S, Pacaud LB, Taran T and Slamon D. Combination of everolimus with trastuzumab plus paclitaxel as first-line treatment for patients with HER2-positive advanced breast cancer (BOLERO-1): a phase 3, randomised, double-blind, multicentre trial. Lancet Oncol 2015; 16: 816-29.

[18] Li X, Gu X, Xu J, Chen L, Li H, Meng D, Bai H, Yang J and Qian J. Sustained clinical benefit of pyrotinib combined with capecitabine rescue therapy after trastuzumab resistance in HER2-positive advanced gastric cancer: a case report. Onco Targets Ther 2021; 14: 3983-3989.

[19] Wang FH, Zhang XT, Li YF, Tang L, Qu XJ, Ying JE, Zhang J, Sun LY, Lin RB, Qiu H, Wang C, Qiu MZ, Cai MY, Wu Q, Liu H, Guan WL, Zhou AP, Zhang YJ, Liu TS, Bi F, Yuan XL, Rao SX, Xin Y, Sheng WQ, Xu HM, Li GX, Ji JF, Zhou ZW, Liang H, Zhang YQ, Jin J, Shen L, Li J and Xu RH. The Chinese Society of Clinical Oncology (CSCO): clinical guidelines for the diagnosis and treatment of gastric cancer, 2021. Cancer Commun (Lond) 2021; 41: 747-795.

[20] Sundaresan TK, Sequist LV, Heymach JV, Riely GJ, Jänne PA, Koch WH, Sullivan JP, Fox DB, Maher R, Muzikansky A, Webb A, Tran HT, Giri U, Fleisher M, Yu HA, Wei W, Johnson BE, Barber TA, Walsh JR, Engelman JA, Stott SL, Kapur R, Maheswaran S, Toner M and Haber DA. Detection of T790M, the acquired resistance EGFR mutation, by tumor biopsy versus noninvasive blood-based analyses. Clin Cancer Res 2016; 22: 1103-10.

[21] Cristescu R, Lee J, Nebozhyn M, Kim KM, Ting JC, Wong SS, Liu J, Yue YG, Wang J, Yu K, Ye XS, Do IG, Liu S, Gong L, Fu J, Jin JG, Choi MG, Sohn TS, Lee JH, Bae JM, Kim ST, Park SH, Sohn I, Jung SH, Tan P, Chen R, Hardwick J, Kang WK, Ayers M, Hongyue D, Reinhard C, Loboda A, Kim S and Aggarwal A. Molecular analysis of gastric cancer identifies subtypes associated with distinct clinical outcomes. Nat Med 2015; 21: 449-56.

[22] Maravelia P, Silva DN, Rovesti G, Chrobok M, Stål P, Lu YC and Pasetto A. Liquid biopsy in hepatocellular carcinoma: opportunities and challenges for immunotherapy. Cancers (Basel) 2021; 13: 4334.

[23] Cancer Genome Atlas Research Network. Comprehensive molecular characterization of gastric adenocarcinoma. Nature 2014; 513: 202-209.

[24] Cai LL, Ye HM, Zheng LM, Ruan RS and Tzeng CM. Circulating tumor cells (CTCs) as a liquid biopsy material and drug target. Curr Drug Targets 2014; 15: 965-72.

[25] Mavroudis D. Circulating cancer cells. Ann Oncol 2010; 21 Suppl 7: vii95-100.

[26] Hofman P, Heeke S, Alix-Panabières C and Pantel K. Liquid biopsy in the era of immuno-oncology: is it ready for prime-time use for cancer patients? Ann Oncol 2019; 30: 1448-1459.

[27] Tseng JY, Yang CY, Liang SC, Liu RS, Jiang JK and Lin CH. Dynamic changes in numbers and properties of circulating tumor cells and their potential applications. Cancers (Basel) 2014; 6: 2369-86.

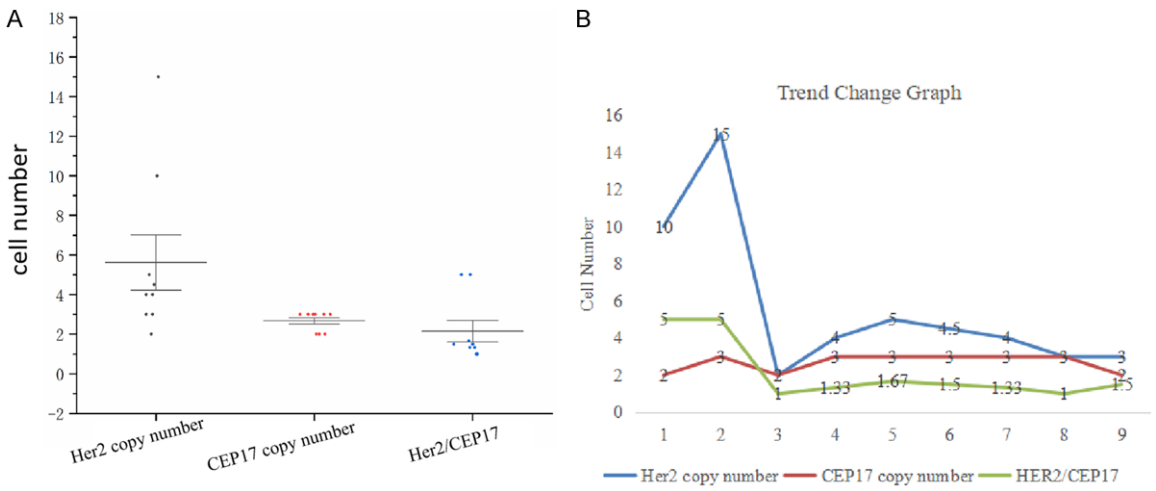

Figure S1. The results of the analysis of mean HER2 copy number/cell, mean CEP17 copy number/cell, and mean HER2 copy number/mean CEP17 copy number. A. Scatter diagram; B. Trend Change Graph.

Table S1. 610 genes panel

Gene list						
ABL1	ABL2	ABRAXAS1	ACVR1	ACVR1B	ADGRA2	AGO2
AKT1	AKT2	AKT3	ALOX12B	AMER1	ANKRD11	APC
AR	ARAF	ARFRP1	ARID1A	ARID1B	ARID2	ARID5B
ASXL1	ASXL2	ATM	ATR	ATRX	AURKA	AURKB
AXIN1	AXIN2	AXL	B2M	BABAM1	BAP1	BARD1
BBC3	BCL10	BCL2L1	BCL2L11	BCL2L2	BCL6	BCOR
BCORL1	BIRC3	BLM	BMPR1A	BRD4	BRIP1	BTG1
BTG2	BTK	CALR	CARD11	CARM1	CASP8	CBFB
CBL	CCND1	CCND2	CCND3	CCNE1	CCNQ	CD22
CD274	CD276	CD70	CD79A	CD79B	CDC42	CDC73
CDH1	CDK12	CDK4	CDK6	CDK8	CDKN1A	CDKN1B
CDKN2A	CDKN2B	CDKN2C	CEBPA	CENPA	CHD2	CHD4
CHEK1	CHEK2	CIC	COP1	CREBBP	CRKL	CRLF2
CSDE1	CSF1R	CSF3R	CTCF	CTLA4	CTNNA1	CTNNB1
CUL3	CUL4A	CXCR4	CYLD	CYP17A1	CYSLTR2	DAXX
DCUN1D1	DDR1	DDR2	DICER1	DIS3	DNAJB1	DNMT1
DNMT3A	DNMT3B	DOT1L	DROSHA	DUSP4	E2F3	EED
EGFL7	EIF1AX	EIF4A2	EIF4E	ELF3	ELOC	EMSY
EP300	EPAS1	EPCAM	EPHA3	EPHA5	EPHA7	EPHB1
EPHB4	ERBB2	ERBB3	ERBB4	ERCC1	ERCC2	ERCC3
ERCC4	ERCC5	ERF	ERG	ERRFI1	ESR1	ETV1
EZH1	EZH2	FAM46C	FANCA	FANCC	FANCD2	FANCE
FANCF	FANCG	FANCL	FAS	FAT1	FBXW7	FGF10
FGF12	FGF14	FGF19	FGF23	FGF3	FGF4	FGF6
FGFR4	FH	FLCN	FLT1	FLT3	FLT4	FOXA1
FOXL2	FOXO1	FOXP1	FRS2	FUBP1	FYN	GABRA6
GATA1	GATA2	GATA3	GATA4	GATA6	GID4	GLI1
GNA11	GNA13	GNAQ	GNAS	GPS2	GREM1	GRIN2A
GRM3	GSK3B	H3F3A	H3F3B	H3F3C	HDAC1	HGF

HIST1H1C	HIST1H2BD	HIST1H3A	HIST1H3B	HIST1H3C	HIST1H3D	HIST1H3E
HIST1H3F	HIST1H3G	HIST1H3H	HIST1H3I	HIST1H3J	HIST2H3C	HIST2H3D
HIST3H3	HLA-A	HLA-B	HLA-C	HLA-DMA	HLA-DMB	HLA-DOA
HLA-DOB	HLA-DPA1	HLA-DPB1	HLA-DQA1	HLA-DQA2	HLA-DQB1	HLA-DQB2
HLA-DRA	HLA-DRB1	HLA-DRB3	HLA-DRB4	HLA-DRB5	HNF1A	HOXB13
HRAS	HSD3B1	HSP90AA1	ICOSLG	ID3	IDH1	IDH2
IFNGR1	IGF1	IGF1R	IGF2	IKBKE	IKZF1	IL10
IL7R	INHA	INHBA	INPP4A	INPP4B	INPPL1	INSR
IRF2	IRF4	IRS1	IRS2	JAK1	JAK2	JAK3
JUN	KAT6A	KDM5A	KDM5C	KDM6A	KDR	KEAP1
KEL	KLF4	KLHL6	KMT2B	KMT2C	KMT2D	KMT5A
KNSTRN	KRAS	LATS1	LATS2	LMO1	LRP1B	LTK
LYN	LZTR1	MAF	MAGI2	MALT1	MAP2K1	MAP2K2
MAP2K4	MAP3K1	MAP3K13	MAP3K14	MAPK1	MAPK3	MAPKAP1
MAX	MCL1	MDC1	MDM2	MDM4	MED12	MEF2B
MEN1	MERTK	MGA	MITF	MKNK1	MLH1	MPL
MRE11	MSH3	MSH6	MSI1	MSI2	MST1	MST1R
MTAP	MTOR	MUTYH	MYCL	MYCN	MYD88	MYOD1
NBN	NCOA3	NCOR1	NEGR1	NF1	NF2	NFE2L2
NFKBIA	NKX2-1	NKX3-1	NOTCH1	NOTCH3	NOTCH4	NPM1
NRAS	NRG1	NSD1	NSD2	NSD3	NT5C2	NTHL1
NUF2	NUP93	P2RY8	PAK1	PAK3	PAK5	PALB2
PARP1	PARP2	PARP3	PAX5	PBRM1	PDCD1	PDCD1LG2
PDGFRB	PDK1	PDPK1	PGR	PHOX2B	PIK3C2B	PIK3C2G
PIK3C3	PIK3CA	PIK3CB	PIK3CD	PIK3CG	PIK3R1	PIK3R2
PIK3R3	PIM1	PLCG2	PLK2	PMAIP1	PMS1	PMS2
PNRC1	POLD1	POLE	PPARG	PPM1D	PPP2R1A	PPP2R2A
PPP4R2	PPP6C	PRDM1	PRDM14	PREX2	PRKAR1A	PRKCI
PRKD1	PRKDC	PRKN	PRSS8	PTCH1	PTEN	PTP4A1
PTPN11	PTPRD	PTPRO	PTPRS	PTPRT	QKI	RAB35
RAC1	RAC2	RAD21	RAD50	RAD51	RAD51B	RAD51C
RAD51D	RAD52	RAD54L	RANBP2	RASA1	RB1	RBM10
RECQL	RECQL4	REL	RHEB	RHOA	RICTOR	RIT1
RNF43	RPS6KA4	RPS6KB2	RPTOR	RRAGC	RRAS	RRAS2
RTEL1	RUNX1	RUNX1T1	RXRA	RYBP	SDHA	SDHAF2
SDHB	SDHC	SDHD	SESN1	SESN2	SESN3	SETD2
SF3B1	SGK1	SH2B3	SH2D1A	SHOC2	SHQ1	SLIT2
SLX4	SMAD2	SMAD3	SMAD4	SMARCA4	SMARCB1	SMARCD1
SMO	SMYD3	SNCAIP	SOCS1	SOS1	SOX10	SOX17
SOX2	SOX9	SPEN	SPOP	SPRED1	SPTA1	SRC
SRSF2	STAG2	STAT3	STAT4	STAT5A	STAT5B	STK11
STK19	STK40	SUFU	SUZ12	SYK	TAF1	TAP1
TAP2	TBX3	TCF3	TCF7L2	TEK	TERC	TERT
TET1	TET2	TGFBR1	TGFBR2	TIPARP	TMEM127	TNFAIP3
TNFRSF14	TOP1	TOP2A	TP53	TP53BP1	TP63	TRAF2
TRAF7	TSC1	TSC2	TSHR	TYRO3	U2AF1	UPF1
VEGFA	VHL	VTCN1	WISP3	WT1	WWTR1	XIAP
XPO1	XRCC2	YAP1	YES1	ZBTB2	ZFHX3	ZNF217
ZNF703						

ALK	BCL2	BCR	BRAF	BRCA1	BRCA2	CD74
EGFR	ETV4	ETV5	ETV6	EWSR1	EZR	FGFR1
FGFR2	FGFR3	FLI1	KIT	KMT2A	MET	MSH2
MYB	MYC	NOTCH2	NTRK1	NTRK2	NTRK3	NUTM1
PDGFB	PDGFRA	RAF1	RARA	RET	ROS1	RSPO2
SDC4	SLC34A2	TMPRSS2				

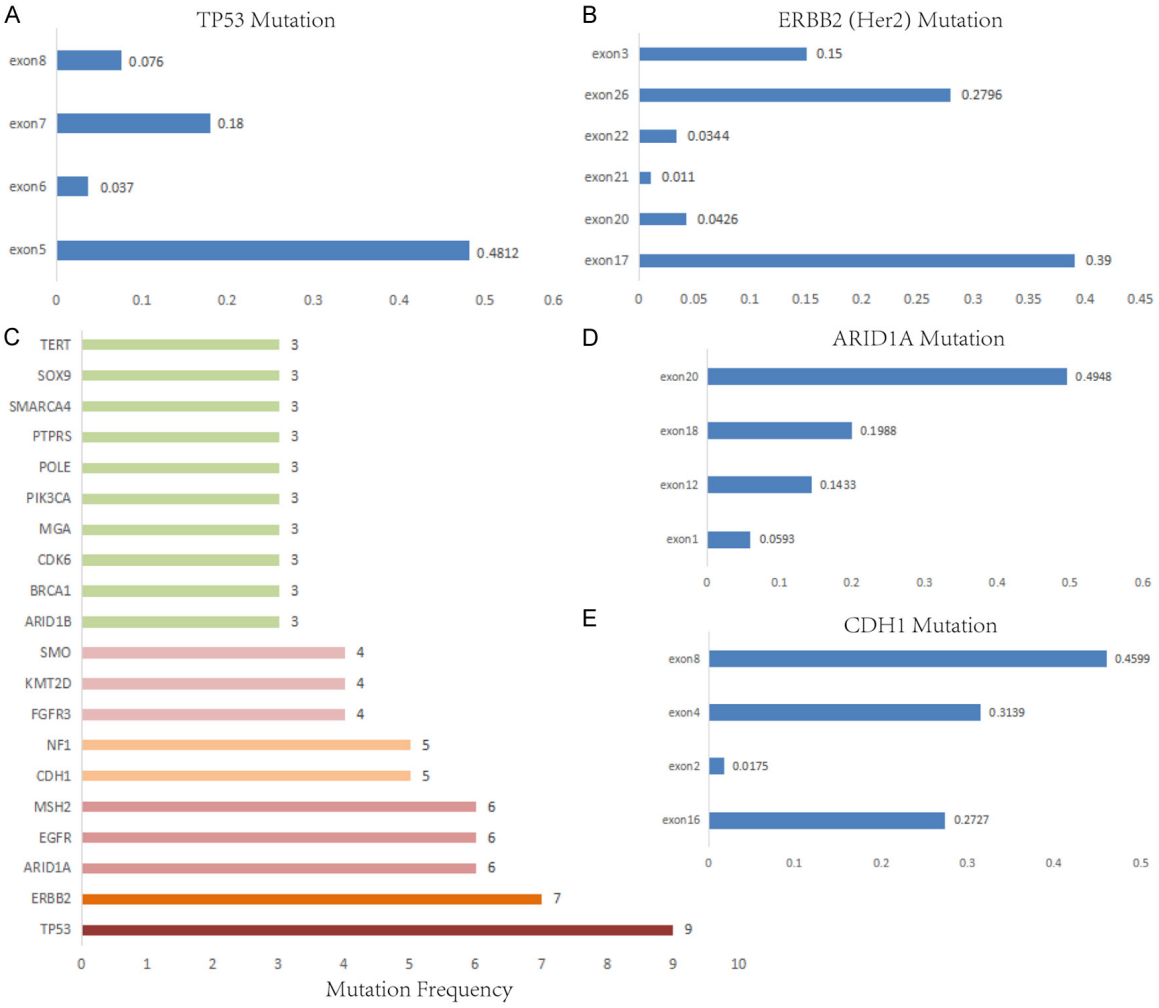

Figure S2. The NGS sequencing of GC clinical samples. A. The main mutation sites of TP53; B. The main mutation sites of ERBB2 (HER2); C. Further sequencing results of gastric cancer CTC-NGS; D. The main mutation sites of ARID1A; E. The main mutation sites of CDH1.

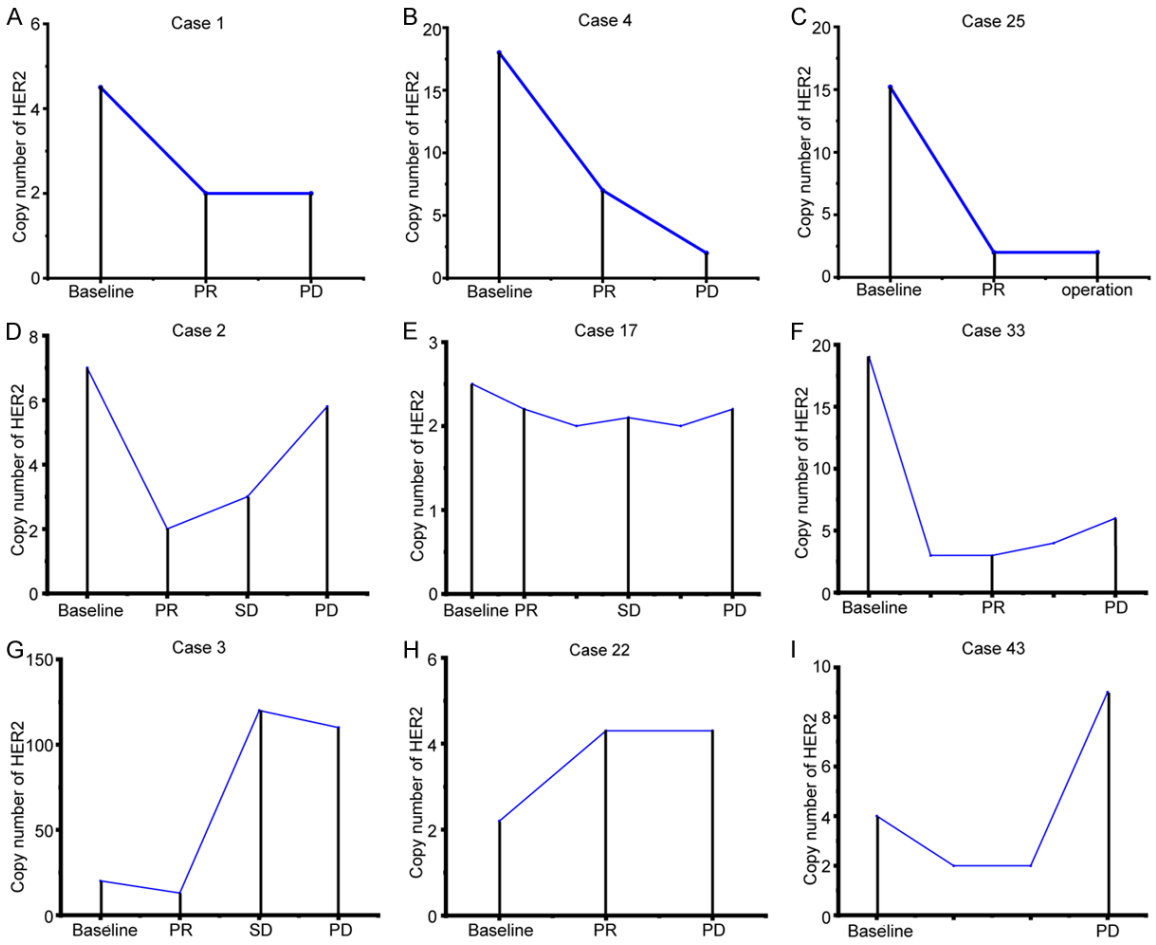

Figure S3. Tracking of enrolled samples, tracking the change in CTC number from Baseline to PR, SD, and PD. A. Case 1; B. Case 4; C. Case 25; D. Case 2; E. Case 17; F. Case 33; G. Case 3; H. Case 22; I. Case 43.

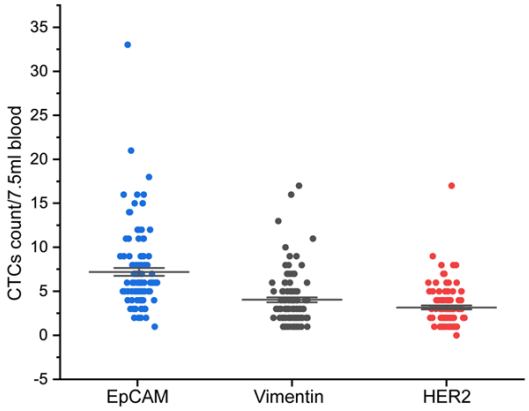

Figure S4. The statistical results of the number of CTC by EpCAM LMB, Vimentin-LMB and HER2-LMB.

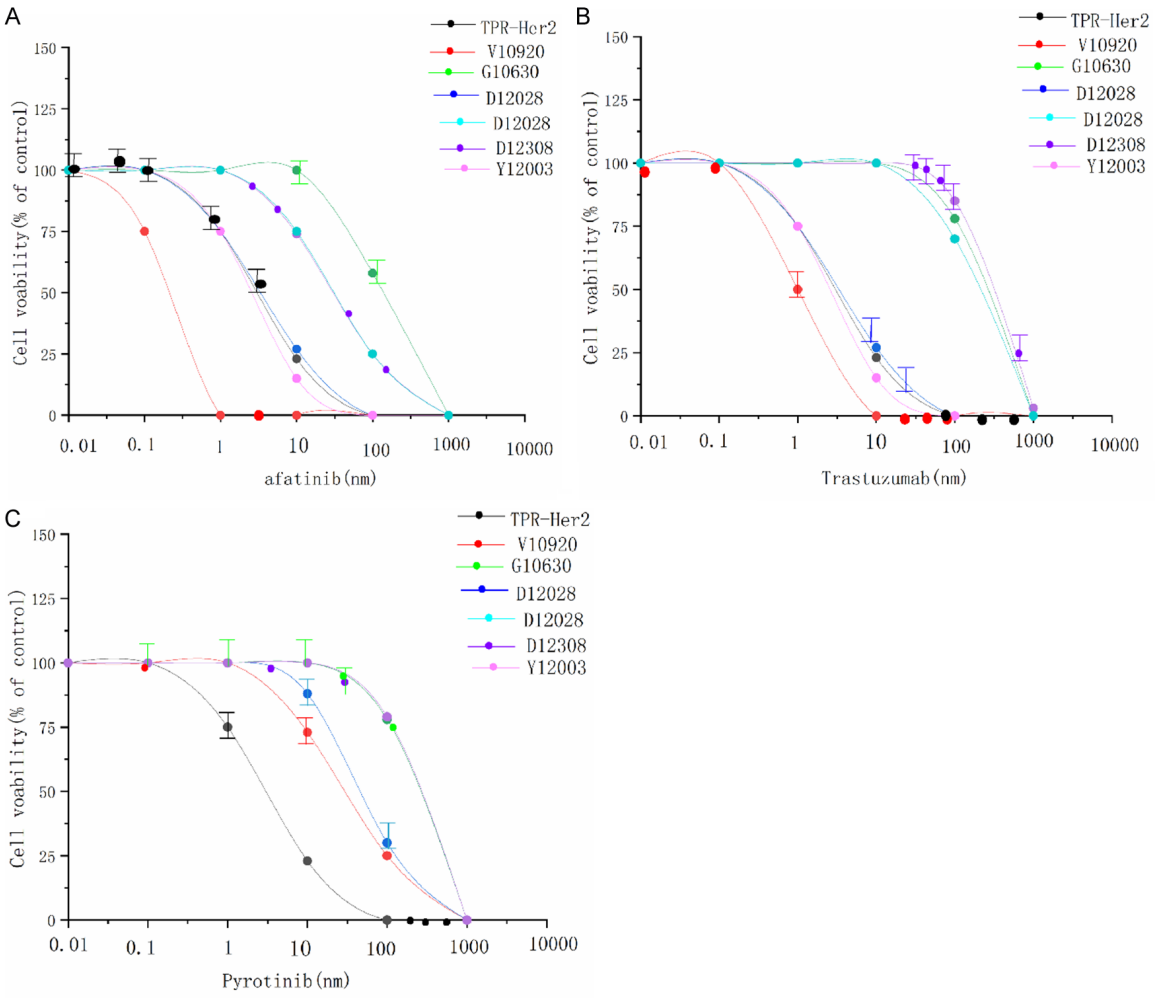

Figure S5. Viability dose-response curves of GC cells exposed to: (A) apatinib, (B) trastuzumab, and (C) pyrotinib.